Light amplification and oscillation in the HeNe resonator

Edwin Ng,[*,1] **Tatsuhiro Onodera,**[1] **Conrad Stansbury,**[2] **and Linda Zhang**[1]

Departments of [1] *Applied Physics and* [2] *Physics, Stanford University*

[*] *Report author: edwin98@stanford.edu*

Compiled March 20, 2015

We investigate the steady-state properties and operation of a laser using a helium-neon (HeNe) discharge tube as the gain medium. We demonstrate that the HeNe plasma is optically active and provides a small-signal, single-pass gain of 15.5 %/m. A confocal optical resonator is then built around the discharge tube and sustained laser oscillation at 633 nm is observed. We measure the saturation intensity of the gain medium as a function of discharge current, and we measure the output power of the laser as a function of its intracavity loss. Some properties of laser resonators in general are also discussed.

OCIS codes: (140.1340) Atomic gas lasers; (14.3410) Laser resonators; (140.4480) Optical amplifiers

1. Introduction

Like their electronic counterparts, the essential components of a laser oscillator are a gain medium, a pump mechanism, and feedback. In the case of gas lasers like the HeNe, the gain medium is a gas through which an electric discharge current (the pump mechanism) is passed. Energetic electrons collide with the gas atoms, promoting them to excited states and producing population inversion. Optical feedback provided by a high-Q resonator built around the enclosed gas then allows circulating light in the resonator to stimulate emission and thus extract optical power from the gain medium.

In a gaseous mixture of helium and neon, the electrons excite ^{3}He atoms to the relatively long lived 2^1S and 2^3S states. It turns out that these states have nearly the same energy as the $3s_2$ and $2s_2$ states of ^{20}Ne (relative to their respective atomic ground states), so interatomic collisions in the gas can efficiently excite the Ne atoms as well. At this point, there are three strong transitions of interest: at 3.39 µm from $3s_2$ to $3p_4$, at 1.15 µm from $2s_2$ to $2p_4$, and at 633 nm from $3s_2$ to $2p_4$. This last transition is the preferred one for visible light operation of the HeNe laser and is the focus of this report. From the $2p_4$ level, fast radiative decay brings the Ne atoms down to the 1s state, from which they relax to the ground state via wall collisions. [1, 2, pp. 121–123]

The quartz-glass Jodon HeNe discharge tube we use is about 40 cm long, with a 3.2 mm bore diameter and filled at a 7 to 1 ratio of ^{3}He to ^{20}Ne, to a pressure of 1.4 Torr. The discharge circuit consists of a cathode and anode inside the tube and a high voltage DC power supply in series with a high-power ballast resistor for current control. A meter reads out the discharge current I_D, which can be tuned from about 4.7 mA to 7.1 mA. The ends of the tube are cut to Brewster's angle (approximately 56°) to minimize reflections for p-polarized light, which has the effect of defining the laser polarization due to mode competition. The discharge tube and its circuitry are mounted inside a box (with holes cut for the optical beam), and it is placed on top of an optical rail setup to facilitate rough alignment of cavity mirrors. [3]

2. Gain medium characterization

For the purpose of characterizing the gain medium, we align a commercial HeNe probe laser (output ∼3 mW) through the discharge tube, using a lens to avoid clipping the probe around the inner bore. By measuring the probe power before and after the enclosed discharge tube (along with ∼0.3 m of free space on both ends), we estimate the single-pass intracavity loss a_0 for a typical resonator setup is 2.5 %. We note some of this loss is due to the non-ideal cut of the Brewster windows—even at optimal probe polarization, some reflection off the input window is observed.

Next, we measure the single-pass, small-signal gain g_0 of the discharge tube, which may in principle depend on I_D. We take g_0 to be the ratio of the probe power with the discharge on to the probe power with the discharge off; both power measurements are taken downstream from the tube, in order to isolate g_0 from a_0. Interestingly, we find no dependence on I_D: the output power remains constant with changing I_D. The observed value of g_0 in this measurement is 6.19 %.

To ensure we are measuring the *small-signal* gain, however, we place a variable attenuator wheel after the probe output and before the discharge tube, in order to measure g_0 with smaller probe powers. Setting I_D constant at 7.1 mA, we vary the attenuation and again record the probe power after the discharge tube, with the current turned alternately on and off. The resulting data shows a very linear relationship between the two power measurements, for probe attenuations spanning two orders of magnitude (unamplified probe powers range from 0.006 mW to 0.955 mW, taken after the tube). A linear least-squares fit to the data estimates the slope to be 6.16 %, consistent with the above measurement of g_0 at maximal probe power. A plot of this data with the fit is shown in Fig. 1 below.

Based on these observations, we take g_0 to be a constant throughout this experiment, with an estimated value of 6.2 %. Given the tube length of 0.4 m, the single-pass, small-signal gain coefficient α of this particular HeNe discharge tube is therefore $\alpha = 15.5$ %/m.

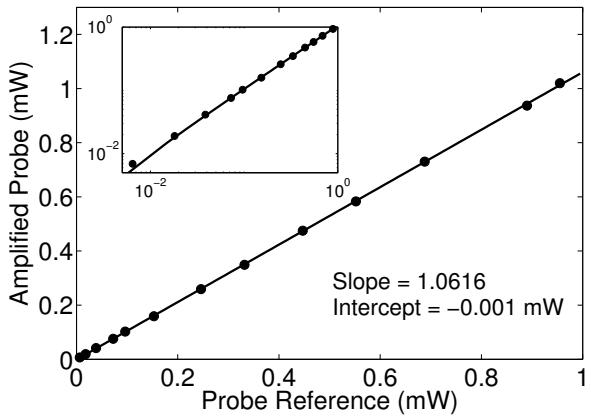

Fig. 1: Measurement of single-pass gain for various probe powers, at $I_D = 7.1\,\mathrm{mA}$. Probe reference is taken after the tube with discharge off; amplified probe is with discharge on. Inset shows the data on a log-log plot, demonstrating linearity across a large range of probe power.

3. Resonator properties

To ensure stability in the laser oscillator measurements that follow, we utilize a symmetric confocal optical resonator design consisting of two spherical mirrors at 633 nm: one, a high reflector (measured loss $< 0.1\,\%$) and the other, a 1% output coupler (measured $T = 1.28\,\%$). Both mirrors have a radius of curvature of 0.5 m and are placed about $L = 1\,\mathrm{m}$ apart on the optical rail setup, nominally centered on the discharge tube.

Rough cavity alignment is performed with the probe HeNe beam, by back-reflecting the probe with the output coupler, followed by the high reflector. Once we achieve lasing operation, the alignment is optimized by iteratively fine-tuning the mirror mounts to maximize the output power. At $I_D = 7\,\mathrm{mA}$, we achieve a maximum output power of 2.02 mW. Over the course of the experiment, however, this drops to 1.93 mW (even with re-optimization); it is not obvious what causes this drop.

Theoretically, the confocal resonator supports a stable TEM_{00} Gaussian mode with $1/e^2$ waist $w_0 = \sqrt{\lambda L/2\pi}$ ($= 0.317\,\mathrm{mm}$ for $\lambda = 633\,\mathrm{nm}$) at the middle of the resonator; the Rayleigh range is $z_0 = L/2$. [2, p. 18] Using a CCD camera placed $z = 31\,\mathrm{cm}$ from the output coupler, we observe a Gaussian mode with a $1/e^2$ spot size of approximately 0.61 mm, consistent with $w = w_0\sqrt{1 + (z_0 + z)^2/z_0^2} = 0.604\,\mathrm{mm}$. We note some observed ellipticity of the spot (eccentricity ~ 0.3) but are unable to discern whether it is an imaging artifact.

Before moving on to experiments involving the laser output power, however, it is interesting to first look at a few *spectral* features of the HeNe laser.

First, we utilize a CCD grating spectrometer (Thorlabs CCS175; 500 nm–1000 nm) to compare the spectral output of the laser against the glow discharge spectrum of the HeNe tube taken from the side, shown in Fig. 2a. Compared to the glow discharge, the laser output is very spectrally pure, with our measurement limited by the spectrometer resolution, quoted as 0.6 nm. The peak of the output occurs at 632.5 nm, which is consistent with the expected operating wavelength of 632.8 nm, to within the spectrometer resolution.

Next, we can also send the laser output into a scanning confocal interferometer (Thorlabs SA200-5B, FSR 1.5 GHz), in order to observe the *longitudinal* modes of the cavity. A trace of such a scan is shown in Fig. 2b, which confirms the existence of multiple longitudinal modes in the laser output, separated by a measured cavity FSR of 145 MHz, consistent with $c/2L = 150\,\mathrm{MHz}$ for the longitudinal modes of the 1 m confocal resonator. Because the width of these modes are comparable to the quoted interferometer resolution of 7.5 MHz, the spectral purity of these modes are again limited by our equipment. We also see from Fig. 2b that there is a distinctive gain profile supporting these multiple longitudinal modes. Thus, the HeNe laser has a gain bandwidth of approximately 1.2 GHz at 633 nm.

Finally, we note that we also achieved lasing with both hemispherical and spherical resonators, but these designs are more sensitive to misalignment and more easily support higher-order modes. For some examples of such higher-order modes, see Fig. 3 below.

Fig. 2: Spectral measurements of the HeNe laser output.

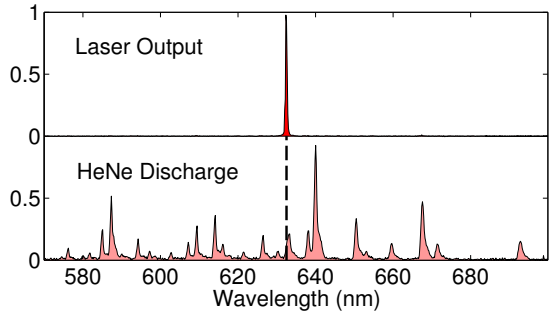

(a) A comparison of the laser spectrum (top, background subtracted) to the HeNe discharge spectrum (bottom). Both spectra are normalized to their peaks. The dashed line indicates $\lambda = 632.5\,\mathrm{nm}$, the observed peak of the laser output.

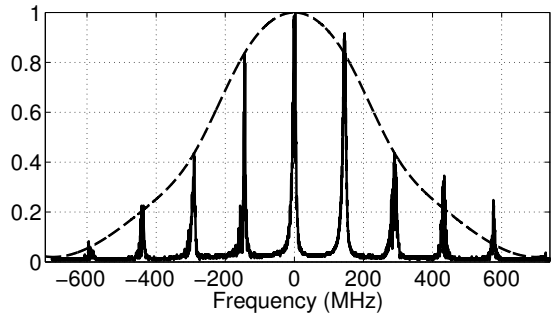

(b) The frequency content of the laser output, as seen by a scanning interferometer. Because of drifts between scans, our calibration using a large-amplitude sweep across multiple interferometer FSRs limits the accuracy of the frequency scale to 5 MHz (systematic). The dashed curve is a qualitative sketch of the HeNe gain bandwidth, inferred from the spectrum envelope. There appears to be a mechanical fluctuation between the 7th and 8th peak.

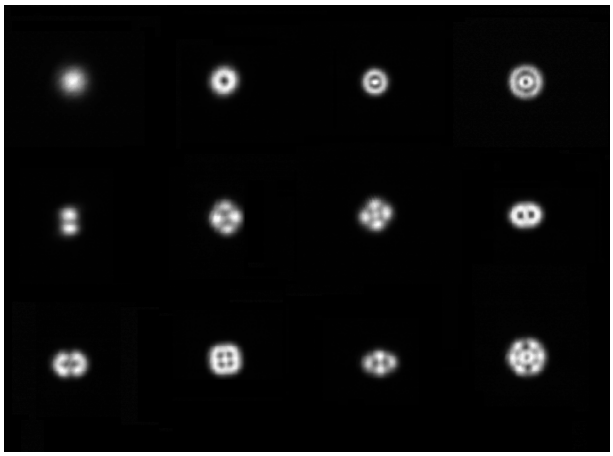

Fig. 3: Examples of modes seen with other resonator configurations (TEM_{00} upper-left). These modes are found using hemispherical and spherical configurations near the edge of stability and are taken using a CCD camera with a focusing lens after the output coupler. Examples of both Hermite-Gaussian and Laguerre-Gaussian modes (and also possibly hybrids) can be seen.

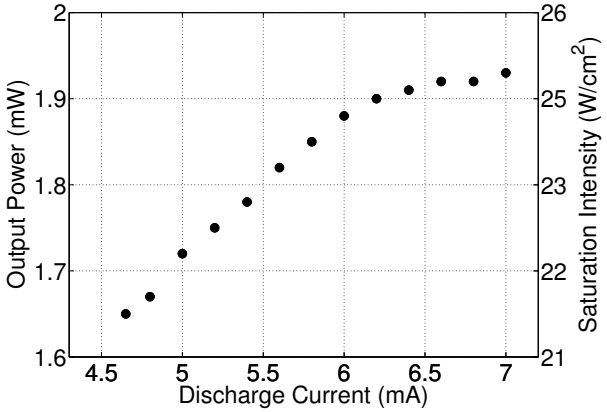

Fig. 4: Plot of laser output power as a function of discharge current. The left axis is the actual measured power, while the right axis is a rescaling according to $\mathcal{I}_{\rm sat} = (160.3)P_{\rm out}/\pi(0.61\,{\rm mm})^2$, as determined by inserting previous measurements into Eq. 1.

4. Steady-state laser operation

Once optical feedback is applied by the resonator, the intracavity power increases due to multiple passes of light through the gain medium. This large intracavity intensity $\mathcal{I}$ saturates the gain medium, and, in the case of homogeneous saturation, reduces the single-pass gain to

$$g = \frac{g_0}{1 + \mathcal{I}/\mathcal{I}_{\rm sat}(I_D)},$$

where $\mathcal{I}_{\rm sat}(I_D)$ characterizes the saturation behavior (i.e., the $-3\,$dB corner) for a given I_D. Note that this equation only applies at each particular point of the gain medium, and we would in principle need to integrate it to find the actual gain. However, in a small-saturation approximation, we can treat the Gaussian beam as a uniform cylinder of effective area $A = \pi w_0^2$, so we may define $P_{\rm sat}(I_D) = \mathcal{I}_{\rm sat}(I_D)A$ and take $\mathcal{I} = P/A$, where P is now the total intracavity power. [4]

Thus, for fixed cavity losses, the intracavity power builds, until the gain is sufficiently saturated to be equal to the losses. This steady-state condition means we set $2g = 2a_0 + T$ (the double-pass gain is equal to the double-pass loss plus the output coupling). We solve for P and note the output power is $P_{\rm out} = (T/2)P$, so

$$P_{\rm out} = \frac{1}{2}T\left(\frac{g_0}{a_0 + T/2} - 1\right)P_{\rm sat}(I_D). \qquad (1)$$

Since we know g_0 is independent of I_D, Eq. 1 suggests that a measurement of $P_{\rm out}$ as a function of I_D is a direct measurement of $P_{\rm sat}(I_D)$, up to a constant factor involving known parameters (i.e., $T = 1.28\,\%$, $g_0 = 6.2\,\%$, and $a_0 = 2.5\,\%$). Such a measurement is presented in Fig. 4, for the range of discharge currents available.

There are actually some subtleties to note when interpreting Fig. 4. In a prototypical laser (say, the three-level system), g_0 generally increases with pump rate R_P, while $P_{\rm sat}$ is usually independent of R_P. For such a laser operating at steady state with fixed losses a, $P_{\rm out}(R_P) \propto g_0(R_P)/a - 1$. Lasing occurs when $g_0(R_p)/a \geq 1$, and the saturation of this requirement is the laser threshold. If $g_0 \propto R_P$ and $R_P \propto P_{\rm pump}$, then we can also define a slope efficiency $P_{\rm out}/P_{\rm pump}$.

This is not the behavior observed here. Instead, we find g_0 is independent of discharge current I_D, while (taking Eq. 1 at face value) $P_{\rm sat}$ non-trivially depends on I_D. More pointedly, if we extrapolate the linear region of Fig. 4 to zero output power, we find "threshold" occurs at $I_D = -8.8\,$mA! Thus, neither threshold nor slope efficiency is well-defined by looking only at I_D.

These observations suggest that the tuning of the output power in Fig. 4 is due to plasma physics in the HeNe discharge tube, rather than rate relations. [2, 5, p. 123] That is, R_P is somehow related to I_D in such a way that, within the tuning range of I_D, R_P (and hence g_0) changes negligibly, while $P_{\rm sat}$ depends sensitively on I_D via some plasma-based mechanism (perhaps modifying the emission/absorption cross-sections). We do not speculate as to the actual physics involved, but these are the most likely implications if we accept that Eq. 1 is a good description of the HeNe laser. Both the assumption of homogeneous saturation and the laser rate equations for a three-level system still hold, but unlike a typical laser system where we have direct control over R_P via $P_{\rm pump}$, I_D is non-trivially tied to the physical parameters going into the governing equations.

Finally, in our last experiment, we directly modulate the cavity loss by inserting a pair of counter-rotating glass plates into the cavity. Since the laser polarization is fixed, the angle of the plates determines their transmittance according to the Fresnel equations, which therefore acts as an variable attenuator/loss element. [6]

To determine the effect of the variable loss on the output power, we modify Eq. 1 as follows:

$$P_{\text{out}} = \frac{1}{2}T\left(\frac{g_0}{a_0 + T/2 + a} - 1\right) P_{\text{sat}}(I_D), \qquad (2)$$

where a is the variable single-pass attenuator loss.

The plates are mounted in a box with holes drilled on the sides and placed onto the optical rail for coarse alignment with the cavity. The angle of the plates is tuned using a micrometer, for which 10 mm translation corresponds to 90° rotation, from normal incidence to grazing.

We note two effects which immediately suggests difficulty in using the attenuator for the desired measurements. First, the vertical position and tilt of the attenuator is critical—small adjustments to placement (∼2 mm) drastically change the output power, even at Brewster's angle. Second, there is a pronounced etalon effect as the attenuator is turned, with one fringe corresponding to less than the smallest tick mark on the micrometer (0.01 mm, or 0.09°). The first issue suggests that the Brewster plates, despite their design, still introduce some deflection of the beam, destabilizing the cavity mode.

We rest one side of the attenuator on a folded cloth that gives the right height to maximize the output power at Brewster's angle. We observe the laser output to drop from 2.02 mW to 1.35 mW as this is done (and as low as 1.10 mW without the adjustments). For our measurements, we use micrometer settings from 4.00 to 6.00, in steps of 0.25, corresponding to angles between 36° to 54° (≈ Brewster's angle), in steps of 2.25°. We attempt to sidestep the etalon issue by dialing the micrometer knob around the desired setting by plus or minus one tick mark, until the fringe maximum is found.

Although the single-pass loss a of the attenuator can be calculated from its geometry and the Fresnel equations, we opt for a more direct characterization of the attenuator by measuring a using the probe beam from before, at the micrometer settings of interest (and using the same technique for the etalon issue). We find losses ranging from 0.64 % (at 54°) to 5.36 % (at 36°).

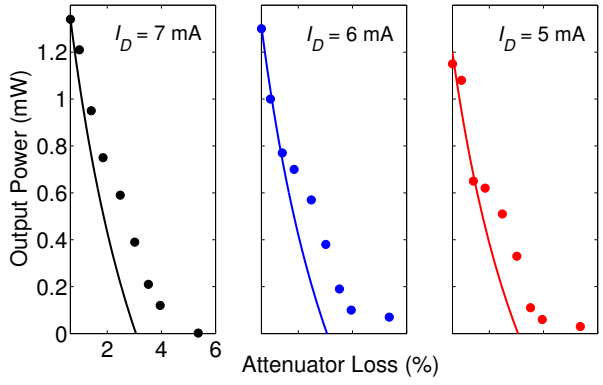

Fig. 5: Laser output power as a function of the single-pass loss of the variable attenuator, for discharge currents of 7 mA, 6 mA, and 5 mA. The solid line indicates a plot of Eq. 2 for $T = 1.28\,\%$, $g_0 = 6.2\,\%$, $a_0 = 2.5\,\%$, and $P_{\text{sat}}(I_D) = (160.3)P_{\text{out}}(I_D)$ as found in Fig. 4.

In Fig. 5, we plot the laser output power as a function of the above measured losses for various discharge currents, alongside the expected behavior according to Eq. 2, given the measurements already performed.

While the overall trend is correct, there is a clear systematic effect which consistently affects the measurements at all values of I_D. In particular, the laser is expected to threshold and cease lasing when $a \geq g_0 - a_0 - T/2 \approx 3\,\%$, but this did not occur: lasing was observed well past $a = 5\,\%$, although at the extreme values of loss, the power output is small and unstable as we pass through the fringes, indicative of near-threshold behavior. (The laser stops lasing at every fringe minimum, and for much larger losses, which we did not record.)

These systematic effects make it difficult to fit the data to Eq. 2 and hence verify Eq. 1 by comparing the fit parameters to the previous, independent measurements of gain, loss, and saturation power. For what it's worth, the first data point at Brewster's angle is interestingly consistent: at $I_D = 7$ mA, for example, Eq. 2 predicts $P_{\text{out}} = 1.34$ mW based on previously measured values and $a = 0.64\,\%$, exactly the observed value when the attenuator is added to the cavity at Brewster's angle. This may have to do with our initial optimization of the vertical position, which was performed at this angle.

5. Conclusions

The HeNe discharge tube is found to be optically active and can function as an amplifier ($\alpha = 15.5\,\%/\text{m}$) at 633 nm. A confocal resonator is built around the discharge tube and laser oscillation is achieved in the TEM_{00} mode. Spectral measurements indicate the presence of multiple longitudinal modes and confirm the spectral purity of the laser output. Control of the discharge current allows tuning of the output power between 1.6 mW and 2 mW, for intra-cavity losses of 2.5 % and a 1.3 % output coupling; measurements suggest the mechanism for such tuning is based on plasma physics rather than modulation of the pump rate. Finally, the cavity loss is controlled with a variable attenuator to study the homogeneous saturation approximation for the HeNe laser; although we are unable to verify the model due to systematic effects, the overall trends in the data are consistent with the model.

References

1. K. Thyagarajan and A. Ghatak, *Lasers: Fundamentals and Applications* (Springer, 2010), pp. 283–285.
2. W. Nagourney, *Quantum Electronics for Atomic Physics* (Oxford University Press, 2010).
3. AP304 Staff, "Experiment 3: The Helium Neon Laser and Laser Resonators" (unpublished lab manual).
4. A.E. Siegman, *Lasers* (University Science Books, 1986), pp. 326–327.
5. R.L. Byer (personal communication with T.O., 2015).
6. K. Bennet and R.L. Byer, "Computer-controllable wedged-plate optical variable attenuator," Appl. Opt. **19**, 14 (1980).